First-Principles Study on Ligand Binding and Positional Disorder in Pentlandite

A First Principles Study On Ligand Binding And Positional Disorder In Pentlandite

Calum. N. Waterson,[a] Julien Sindt, [a] Jun Cheng,[b] Peter A. Tasker, [a] and Carole. A. Morrison [a,*]

[a] The School of Chemistry and EastCHEM Research School, The University of Edinburgh, King's Buildings, David Brewster Road, Edinburgh, EH9 3FJ, UK.

[b] Department of Chemistry, University of Aberdeen, Aberdeen, AB24 3UE, UK.

Abstract

Density functional theory, in conjunction with a cluster expansion model, has been used to study the structure and stability of the positionally disordered iron-nickel sulfide mineral pentlandite (Pn), $(Fe, Ni)_9S_8$, with results indicating heterogeneous nearest neighbour metal contacts are more energetically favourable than homogeneous contacts. The virtual crystal approximation was also explored as a means to address positional disorder, but while reliable results could be obtained for the bulk model, the same was not true for the surface, as local distortions which affected the surface model energies could not be reproduced. We also address the binding of ethyl xanthate ($CH_3CH_2OCS_2^-$), water and hydroxide to the [111] Pn surface to better understand the mode of action of industrial xanthate flotation agents. In order to model anionic ligands bound to a periodic boundary condition surface we propose applying a correction derived from the surface work function to remove the additional charge introduced by the ligand. The results obtained from the ligand binding studies indicate that while an ethyl xanthate collector could readily displace up to a full monolayer of water per unit cell, it is likely that Fe-enriched surfaces will bind xanthate in competition with the hydroxide anion, whilst a Ni-enriched surface will preferentially bind hydroxide anions over xanthate.

Keywords: **DFT, pentlandite, ethyl xanthate, froth flotation, virtual crystal approximation, cluster expansion, surface work function.**

1.0 Introduction

The mining, recovery and processing of Platinum Group Minerals (PGMs) is a multi-billion dollar industry. The Bushveld Igneous Complex in South Africa contains approximately 75% of the world's platinum and 50% of the world's palladium reserves, which are often present as sulfidic ores and associated alongside considerable quantities of base metal sulphides such as pyrite (FeS_2), pyrrhotite ($Fe_{(1-x)}S$ (x=0-0.2)) and the mixed iron/nickel mineral pentlandite $(Fe,Ni)_9S_8$ (Pn),[1] which can itself be a

* Corresponding author. Email: c.morrison@ed.ac.uk

rich source of PGMs with some recorded samples containing up to 12.1 wt% Pd[2]. The ore feed as it comes from the mines has an extremely low PGM concentration (*ca.* 1-3 ppm), so there is a requirement to separate and concentrate PGMs from commercially less valuable minerals, prior to the leaching or smelting stages.

Separating the PGMs from other minerals is usually achieved by froth flotation,[3,4] which operates by aerating a finely-ground ore slurry in a series of agitated tanks. Selective ligands, called mineral collectors, are added to bind to the target mineral surface via chemi- or physisorption. Collectors are typically small organic anionic surfactants, such as ethyl xanthate ($CH_3CH_2OCS_2^-$), that possess an anionic head group to bind to the metal ions on mineral surfaces, while the aliphatic tail renders the surface hydrophobic, facilitating bubble attachment. In this way, mineral particles rise through the tank to form a froth which is mechanically separated for further processing.

Studying the mode of action for collector ligands with mineral surfaces is of major industrial interest,[5] and an area in which some insight can be achieved from computational modelling. The work is challenging, however. High accuracy modelling of the two-phase collector/mineral system requires a first principles condensed matter approach[6], with plane-wave density functional theory (DFT) being the most tractable solution, but this places a restriction on the size of atomistic models that can be processed. Specific to this work was the decision to model pentlandite, which has value as a primary source of Ni, and tends to be preferentially collected over PGMs in the froth floatation process. Pentlandite displays positional disorder of its Fe and Ni sites, which significantly complicates the task of defining a working surface, cleaved from a suitable solid state model, upon which to study ligand binding. Within the ultrasoft pseudopotential method there exists a possible solution in the virtual crystal approximation (VCA)[7], a technique derived to account for static positional disorder and stoichiometric variance in crystal structures. Here a disordered lattice position is replaced with two or more (non-interacting) pseudoatoms, which interpolate between the possible occupants of the site. While this method necessitates the neglect of local structure variation around the pseudoatoms, it has been successfully applied in a number of solid state studies[8,9]. The ability of the VCA method to generate reliable bulk, surface and ligand/surface binding models with high positional disorder is investigated in this paper.

Another approach to dealing with metal site disorder is to parameterise a cluster expansion model. This relates the total energy of a bulk lattice to the species occupying the metal sites by use of a network of pairwise (or higher order) lattice sites and associated interaction constants, which are derived by fitting the cluster expansion to the total energies obtained from a training set of explicitly-defined DFT simulations. A well-parameterised cluster expansion Hamiltonian then allows the

application of a Monte Carlo approach to find the global minimum-energy bulk structure. Moreover the cluster interaction constants allow information to be gleaned regarding the nature of the metal…metal contacts themselves, specifically whether homogeneous (i.e. Fe…Fe or Ni…Ni) or heterogeneous (Fe…Ni) neighbouring metal contacts in the Pn disordered lattice are more likely to be energetically favoured.

A second modelling challenge in this work is the need to bind anionic ligands to the surface model. Placing a negatively charged ligand into a periodic system creates a charged supercell which lacks a well-defined energy.[10] Herein we offer a solution by calculating a correction defined *via* the surface work function that corresponds to the energy required to remove an electron from the mineral surface, thereby returning the model to an effectively charge zero state. The justification for this stems from the fact that the Pn mineral surface is metallic, and thus the charge introduced from the anionic ligand will dissipate (and be effectively diluted) through the slab.

Finally, as sulfide mineral flotation occurs in aqueous media under fairly basic conditions[4], water and hydroxide ions will compete[11] with the collector ligand to bind to the mineral surface. A full *ab initio* treatment of the interfacial water environment involves too many degrees of freedom to be tractable on a reasonable timescale. In this work we address surface binding competition in a more general way by considering the binding of an increasing surface coverage of water molecules, from one molecule per unit cell to a full monolayer. We also consider the binding of a single hydroxide fragment to the Pn mineral surface in order to estimate the initial energetic barrier that the collector ligand would have to overcome in order to bind to the bare mineral surface.

The paper is laid out as follows. In the methods section we first describe the computational models used before moving onto techniques for dealing with positional disorder in bulk and surface Pn models, in which we describe both the VCA and cluster expansion methods. Next we describe the building and assessment of surface models and describe the method used to calculate binding of a formally negatively charged ligand to a mineral surface *via* the surface work function correction. In the results and discussion section we first compare and contrast VCA and explicit Pn bulk models and follow this with the results obtained from the cluster expansion method. We then use the surface work function correction to calculate binding energies for ethyl xanthate, water and hydroxide ligand to the surface of Pn.

2.0 Methods

2.1 Computational details

All geometry optimisation calculations were carried out using the plane-wave DFT code CASTEP[12], version 7.02. The PBE exchange-correlation functional[13] was used, along with a plane-wave basis set with an energy cut-off of 550 eV, which demonstrated convergence to within 0.2 meV/atom. Ultra-soft pseudopotentials[14] were generated 'on-the-fly'. A k-point grid was generated using the Monkhorst-Pack scheme[15] set to 4 x 4 x 1 for all calculations, representing a k-point sampling spacing of no greater than 0.015 $Å^{-1}$. The convergence tolerances for force, ionic displacement and energy were 0.05 $eVÅ^{-1}$, 0.001 Å and 0.01 meV/atom, respectively.

The bulk unit cell parameters and atomic positions of Pn were set at the values determined by Pearson *et al*,[16] which were obtained from the mineral crystallographic database MINCRYST.[17] These cell parameters were **a** (= **b** = **c**) = 10.03 Å, α (= β = γ) = 90° and space group Fm-3m (#225). The bulk unit cell contains a total of 36 metal atom sites, corresponding to 4 octahedral sites and 32 tetrahedral sites. A powder neutron diffraction study on a synthetic Pn sample (which had been annealed at 150 °C for 3 months) suggested a 53(2) % Ni occupancy bias for the octahedral sites and 48(2) % occupancy bias for the tetrahedral sites.[18] A Mössbauer spectroscopy study indicates that the Fe octahedral sites are probably divalent and express an isomer shift intermediate between that for a high and low spin state.[19] The same study suggests that the Fe tetrahedral sites probably carry oxidation state zero. No information appears to be known regarding the oxidation states for the Ni sites. Experimentally, Pn is reported to be non-magnetic[20] and thus has net zero spin, although this does not rule out the possible existence of antiferromagnetic spin polarised states. The problems associated with the computational modelling of Pn are therefore two-fold: firstly, to identify if there are any local correlations in Ni and Fe distribution; secondly, to determine likely oxidation states and spin states for the metal sites. In this work we focus purely on the first problem. To this end, all calculations reported in this paper relate to spin-restricted wavefunctions; we have not pursued the use of DFT+U functionals[21, 22] which are known to be important for correcting the over-delocalisation of electrons observed in condensed matter transition metal systems by pure DFT functionals,[23, 24] and are thus important in work where in-depth knowledge of the oxidation states and spin states is sought.

The final working surface adopted (see below) had a surface unit cell with dimensions **a** = **b** = 14.18 Å, **c =** 35.00 Å, α = β = 90°, γ = 120° when cleaved from the Pn bulk unit cell. This model was used to calculate surface energies. Note it is possible to half the **a** and **b** vectors of the model without losing structural information except for the symmetry of the original bulk unit cell, implying that the symmetry of the original bulk unit cell requires a 2×2 supercell of the surface periodic unit cell to fully describe the identity distribution of its metal sites. For this reason, when a VCA bulk unit cell (in which all the metal atom sites are equivalent) is cleaved it produces a surface unit cell with half the **a, b**

dimensions, comprising 18 metal atom sites. This distinction is important as the smaller Pn surface unit cell was used in the ligand binding studies to reduce the computational cost. This model presents three metal sites for ligand binding, allowing up to three water molecules or hydroxide ions to be bound, but only one xanthate ligand as this will require two metal sites to bind in a bridging fashion. Whilst this makes for an attractive system size for computational modelling work, the issue of whether this is a realistic representation of surface coverage requires discussion. From electrochemical and surface enhanced Raman spectroscopy (SERS) measurements it is generally accepted that ethyl xanthate monomers chemisorb to the surfaces of minerals, and then undergo an oxidative dimerization reaction to form the dixanthogen species, which are thought to form physisorbed multilayers above the chemisorbed monomer.[25 , 26, 27] The extent of surface coverage by the collector ligand appears not to be reported in the literature, however. But since in this work we are interested in modelling the chemisorbed binding of the monomer state only, the number of available binding sites in the proposed models seems reasonable for the task at hand. Note however, this model is only large enough to permit adsorption of one ligand onto one surface; to adsorb onto both surfaces would require the **c** vector to at least double in length, which would render the task extremely compute-heavy. This raises the prospect that the asymmetric ligand+surface models will carry a dipole, which in turn could further polarise the system. However, the dipole correction to the total energy, as calculated using the Neugebauer and Scheffler scheme[28] (implemented in CASTEP 8.0) is small, less than 5 meV per unit cell (see Supporting Information, SI1).

Energies of the optimised ligand models of ethyl xanthate and a hydroxide ion were obtained by optimising one charged ligand molecule inside a cubic unit cell of dimension of at least 30 Å; for water the unit cell size was restricted to 20 Å. Convergence of total energy with unit cell dimensions for the anionic ligands is explored in the Supporting Information, SI2.

2.2 Positional disorder in Pn bulk and surface models

The configurational disorder of metal sites in Pn generates a large number of different bulk and surface metal distributions. One method for solving the issue of a large number of different possible bulk and surface conformations is to adopt the virtual crystal approximation (VCA). This operates by replacing the external potential term $\hat{V}_{ext}$ in the Hamiltonian of each explicit metal atom with a new external potential, which interpolates between the external potentials of all possible site occupants. For Pn this means that all metal sites (either bulk or surface) are replaced with pseudoatoms with the

properties of a 1:1 mix of iron and nickel. Thus just one VCA model can be used to account in a generalised way for all variants with this metal occupancy.

The literature generally recommends that the VCA method is thoroughly benchmarked before use.[10,11] To this end comparisons were made between VCA models and a selection of randomly generated models with explicit metal site occupancy (referred to throughout as 'explicit' models) at three different stages: comparison of optimised bulk, surface and ligand-binding systems. For bulk systems atomic displacements observed following optimisation were compared; for surfaces and for ligand binding comparisons were made on the basis of surface energies and ligand binding energies, respectively.

An alternative to VCA is to generate a cluster expansion expression which relates the total energy of a Pn bulk unit cell to the metal site identity distribution. All neighbouring metal-metal interactions in the Pn bulk below a reasonably long 6 Å cut-off were considered. The high symmetry present in Pn results in only five unique metal-metal interactions within this cut-off [labelled 1-5, see Figure 1, with corresponding bond lengths shown in Figure 1(b)]. Metal site identity is controlled by the parameter σ, which is set to +1 to indicate Fe and -1 for Ni. Thus if two ions occupying neighbouring sites *i* and *j* are of the same species $\sigma_i\sigma_j$ will return a value of 1, and -1 otherwise. The five metal-metal site pairs, including interactions across periodic boundaries, were documented in a separate neighbour list for each interaction along with their degeneracies, and ascribed a value of $\sigma_i\sigma_j$ which were then summed. Each site pair interaction will make a separate contribution to the total energy and so a weighting parameter J_n for each is required. In this way we can define the total bulk energy E_T of any bulk Pn model as:

$$E_T = E_0 + \sum_{n=1}^{5}\left[J_n \sum_{i,j} \sigma_i\sigma_j\right] \qquad (1)$$

where E_0 is a constant baseline energy term. We constructed ten explicit Pn bulk models (labelled A-J) whose metal distributions were chosen randomly (see Supporting Information, SI3) and found their total energy E_T. This represents the training data set, against which the baseline energy E_0 and weighting constants J_n were fitted.

2.3 Definition and testing of surface models

Before dealing with positional disorder in the Pn surface, a generalised working surface was defined using the surface energy as a metric for stability. This was calculated as the difference in the total

energies of a surface slab model (E_{surf}) and a representative bulk model (E_{bulk}) from which the surface has been cleaved containing the same number of atoms in the same stoichiometric mix[29]. This value was then divided by the exposed surface area (A) of the slab model, as shown in equation 2.

$$E_s = \frac{E_{Surf} - E_{Bulk}}{A} \quad (2)$$

It should be noted that the slab has two surfaces, top and bottom, and ideally both should be the same, otherwise the energy obtained will represent a mix of energetic contributions from both surfaces.

For the bulk crystal structure Pn, a number of possible surface models were generated by cleaving along the three low Miller index planes [100], [110] and [111] and varying the point of surface termination (see Supporting Information, SI4). Each surface model thus generated was given a minimum slab depth of 10 Å so as to provide a central 'bulk-like' region to separate the two identical exposed surfaces sufficiently. The ratio of metal-to-sulfur sites was counted for each surface termination model on each Miller index face and compared to the ratio of bulk metal-to-sulfur sites; any model which did not match the bulk ratio was discounted as they are not energetically comparable.

Of all models so generated, only one met the ratio requirement, the metal-terminated surface on the [111] cleavage plane (see Figure 3, Supporting Information SI4, and also Figure 6), which consists of metal sites sitting slightly elevated from the mineral surface and forming threefold hollows interspersed with sulfur ions. Interestingly, this surface mirrors the two 4- and 5-coordinate sulfur sites reported from an X-ray photoelectron spectroscopy study of near-pristine natural pentlandite. [30] While this sets the general structure of the surface model (herein defined as the 'working surface'), the issue of metal site identity still remains. To this end, the ten explicit random Pn bulk model (labelled A-J) already defined to parameterise the cluster expansion expression were cleaved along the [111] Miller Index plane, as was the lowest energy Pn bulk model subsequently found by the cluster expansion expression, and the general VCA bulk model. Thus the surface energies for a total set of twelve surface models were pursued. These represent ideal surfaces; the effects of e.g. surface reconstruction cannot be pursued with models of this size.

2.4 Calculating ligand binding energies

Binding energies are normally calculated from the difference in total energy between a ligated surface [L+S] model and the sum of the total energies for the unbound surface [S] and the unbound ligand [L].

An issue arises however if the ligand to be bound to the surface is an anion, as the resulting periodic system of charged unit cells lacks a well-defined energy per cell[10]. Reliable total energies can be calculated for $[\mathrm{L}]^{-}$, provided the ligand-only model is placed in a sufficiently large unit cell to negate finite-size effects, and the Makov-Payne correction scheme[31] can be applied to aid the energy convergence process. The total energy of $[\mathrm{L}+\mathrm{S}]^{-}$ cannot be calculated in this way, however, as the unit cell vectors have to increase by integer units, which quickly becomes prohibitive. A workaround can be found, however, by recognising that the calculated electronic density of states plot for the bare slab is metallic (see Supporting Information, SI5), so the charge introduced from the ligand will delocalise into the band structure sitting at the Fermi level. (Note this metallic character discounts the use of other energetic correction schemes[32] which have been developed to model localised charged defects within semiconductors and ionic crystals). Moreover, the adsorption of xanthate onto a mineral surface is known from experiment to be an oxidative process (ref).[33] The question then becomes whether the work required to remove the extra electron (via the surface work function correction, ϕ) would be best calculated for the $[\mathrm{L}+\mathrm{S}]$ system or for $[\mathrm{S}]$. Whilst the former would be desirable (and indeed the presence of the adsorbed ligand may alter the work function),[34] the practicalities of this option are severely limited due to the large model sizes required to generate a stable background coulombic potential for this system. The more tractable solution is therefore to remove the electron from model $[\mathrm{S}]$. In practise, the surface work function $\phi_{[S]^0}$ is calculated by subtracting the Fermi energy for the neutral surface model $[\mathrm{S}]^0$ from the negative of the coulomb potential (V_{pot}), averaged over the stable region in the vacuum gap[35] (see Figure 5):

$$\phi_{[S]^0} = \left(-V_{pot}\right) - E_{Fermi}. \tag{3}$$

A practical scheme to calculate the binding energy for a singly charged anion on a surface can then be calculated using the following expression:

$$E_B = ([\mathrm{L}+\mathrm{S}]^0 - \phi_{[S]^0}) - ([\mathrm{L}]^- + [\mathrm{S}]^0) \tag{4}$$

The binding of ethyl xanthate to the working surface of Pn was modelled using both the VCA and atom-explicit models. Starting with the VCA surface, the ligand was docked onto the surface *via* the thiol head group in either a single (*i.e.* with only one sulfur atom addressing the surface), or bridging (*i.e.* with both sulfur atoms addressing different metal ions on the surface, see Figure 2) geometry. The later docking arrangement was the most stable, and all subsequent xanthate binding calculations pursued this geometry exclusively. Following optimisation, the VCA pseudoatoms in the slab were

then exchanged for explicitly (and randomly) defined Fe or Ni ions, while maintaining an overall 1:1 ratio of Fe:Ni. A total of ten models (labelled 1 to 10) were investigated[36].

Any investigation into the effects of ligand/surface binding for a froth flotation application should take into account desolvation of the ligand and surface. Neither are straightforward to achieve without explicit treatment of water molecules, which comes with considerable computational cost. Whilst an estimate of ligand desolvation energy could be obtained, for example, by application of the solvent polarizable continuum model (PCM)[37], this is only a partial solution, as it is reasonable to assume that only the polar binding head-group becomes desolvated upon binding to the mineral surface. Calculating desolvation energies of the surface is also complex, as removal of water from the mineral surface should be into bulk water, not a vacuum layer. It is also reasonable to expect that the work function $\phi_{[S]^0}$ will be dependent upon the presence of water. Previous work by Cheng *et al*[38] showed that a solvated work function for a water monolayer in contact with TiO_2 gave good equivalence to that derived from a full bulk water/surface model. However, the challenge with adopting this procedure for the [111] Pn mineral slab lies in obtaining equivalent water monolayer geometries on both the top and bottom surfaces; any variation in geometry significantly affects the vacuum electrostatic potential, and hence the ability to obtain a stable work function.

In the face of this complexity, some of the effects of solvation in the computational models were instead estimated through simple competitive site binding, by determining the binding energies of both individual water molecules and hydroxide anions, as well as a monolayer of water molecules on relevant surfaces. The modelling of a water monolayer was achieved by considering an increasing number of water molecules (oxygen atom pointing down) to the metal ions on the mineral surface in the 'on-top' orientation (such that an axis bisecting the H-O-H angle was perpendicular to the surface; this binding arrangement has been shown to be more energetically favourable on pure metal surfaces than one where water molecules bridge metal atom sites[39,40]). As there are three exposed metal sites per unit cell these coverages are labelled '1/3', '2/3' and 'full'. It was expected that following optimization the H_2O molecular plane would drop to be almost parallel to the surface[39]. Repeat calculations were performed for higher surface coverage models, with the molecular planes of the different water molecules parallel and perpendicular to one another, to ensure that the lowest energy conformation was achieved. The hydroxide fragment was addressed oxygen atom 'down' into the on-top position of the metals on the mineral surface, with the oxygen-hydrogen bond axis parallel with the surface normal.

3.0 Results and Discussion

3.1 Comparison of VCA and explicit bulk models

Atomic displacement data for the optimisation process of the Pn VCA bulk and explicit bulks A-J, compared to the input crystallographic coordinates, are given in the Supporting Information (Table S7, SI7). They show that the explicit model atoms moved (on average) 0.07 Å, compared to 0.05 Å from the VCA model, indicating that the explicit models experience slightly greater local distortions in the lattice than the averaged VCA model (note the maximum deviation from the experimental structure found for any atomic site was 0.33 Å and 0.27 Å for the explicit and VCA models, respectively). Overall, however, the differences between the modelling approaches appear to be quite small, and so on the basis of bulk geometries, the general VCA model is broadly similar to the explicit model results.

3.2 Cluster expansion models

The $\sum_{i,j}\sigma_i\sigma_j$ terms for all ten explicit bulk models A-J are presented in the Supporting Information, SI8, alongside their predicted total energies and actual total energies , E_T, as derived by DFT geometry optimisations. The two sets of energies are also shown as a correlation plot in Figure 4, where an R^2 fit to a $y = x$ line of 0.9872 testifies to a good performance by the six-parameter cluster expansion Hamiltonian in reproducing the DFT optimised energies. Values for the short-contact J_n interaction parameters and baseline energy term E_0 (obtained by a least squares approach[41]) are shown in Table 1, alongside their 'power ranking', obtained by taking their respective degeneracies into account. From this it was found that interaction J_3 imparts the biggest impact on the total energy, followed by J_2,J_1,J_5 and J_4 in that order. Given that four of the five J_n parameters are positive numbers this suggests that the total energy of the Pn unit cell as expressed by equation 1 will be minimised if neighbouring metal sites are occupied by non-identical ions (i.e. the $\sum_{i,j}\sigma_i\sigma_j$ terms are negative). Thus the cluster expansion expression suggest that more stable bulk models are obtained when the metal ions in the lattice are heterogeneously dispersed. However, we stress that the training set of DFT optimised structures have been derived from spin restricted wavefunctions; whether these correlations hold in a spin-polarised environment, and with more rigorous DFT+U functionals to explore specific metal site oxidation and spin state will require further investigation.

Inserting values for E_0 and J_1-J_5 into Equation 1 permitted the calculation of a predicted total energy for any metal distribution in a Pn bulk unit cell, provided the associated $\sum_{i,j}\sigma_i\sigma_j$ terms can be determined. Using this parameter set a Monte Carlo pair-swapping algorithm was used to efficiently sample the $\binom{36}{18}$ possible metal occupations in the Pn mineral bulk to find the global lowest-energy Pn structure. The resulting structure was subsequently confirmed as the lowest energy structure in the set by a DFT geometry optimisation calculation, which returned a total energy value some 0.4 eV

lower than the most stable randomised bulk model. The structure of the lowest energy bulk unit cell displays a reasonably high degree of symmetry, belonging to space group *P*cma [see Figure 1(c) and (d); atomic positions, alongside the explicit bulk models A-J, are given in the Supporting Information, SI3]. This model supports 50 % Ni occupancy at both the octahedral and tetrahedral sites, in agreement with the neutron powder diffraction study on a synthetic Pn sample quoted earlier [53(2) % Ni occupancy of the octahedral sites and 48(2) % of the tetrahedral sites].[18] Note however, this computational structure search was restricted to just the local metal…metal identity correlations occurring below a 6 Å cut-off radius. This is sufficient to cover the length scale of the crystallographic unit cell comprising 36 metal sites, and as this model comprises only 4 octahedral sites the close match with experiment is not so surprising. Moreover, whilst a low energy ordered model has been found computationally, the lack of any ordered model arising from diffraction studies must point towards the absence of any long-range metal…metal identity correlations. To explore the longer length scale by a cluster expansion route would, however, require the parameterisation of more *J* coupling values to account for those longer correlations, which in turn would necessitate the use of larger unit cell DFT training simulations. The problem quickly becomes intractable. The work performed here on the single unit cell representation does, however, give new insight into the nature of the set of closest metal…metal contact interactions, which on the basis of energetics point towards heterogeneous interactions being favoured over homogeneous ones.

3.3 Comparison of VCA, explicit and cluster expansion model surfaces

The surface energies for the VCA working surface, the ten explicit working surfaces cleaved from the bulk models A-J, and the surface cleaved from the cluster expansion bulk model (labelled 'C.E. surf') are presented in Table 2 along with the total number of iron and nickel ions in each 'layer' of these surface models (as described in Figure 6). The model total energies used to calculate the surface energies presented in Table 3 are given in the Supporting Information, SI9. While the top and bottom surfaces of the slab are identical with respect to a general metal or sulphur site, the metal occupancies will no longer be identical when a random species (Fe or Ni) is assigned to any given metal site. This limitation could be fixed by increasing the slab thickness until it reaches the next completely identical working surface, but the computational cost of this is prohibitive. The lack of equivalent surfaces top and bottom is not a major issue, it simply means that the reported surface energy for any explicit atom model will be an average of the surface energies for both.

The results in Table 2 indicate that the [111] working surface is stable for all models, with the VCA approach predicting the most stable result; this result is anomalous, however, as the VCA approach

fails to recreate local distortions around the different metal ions adequately (see Figure 6), or the appropriate degree of surface relaxation (indeed VCA surfaces expand slightly during optimisation, see the Supporting Information, SI10), and thus retains a structure much closer to the bulk model. All atom-explicit models (A-J and C.E. surf) display significant local distortions. Some are shown graphically in Figure 6. From this we conclude that the VCA cannot be applied reliably to calculate surface geometries and energies for Pn.

The cluster expansion surface model displays a surface energy of 1.38 Jm^{-2}, which lies outside the range defined by explicit models A-J, suggesting that the most stable bulk model does not give rise to the most stable surface.

Whilst acknowledging that the number of surface models studied is small relative to all possible combinations of metal occupancies, analysis of the distribution of Fe and Ni positions suggests that those models which display an excess of Ni ions on the surface (C and J) tend to have lower surface energies than those with an excess of Fe ions on the surface (A, D and CE Surf). There is also a cluster of models with similar surface energies (E,F,G,H & I at 1.16-1.19 Jm^{-2}) which have no surface metal excess, or their excesses cancel. However, evidence from experiment suggests that in an oxidising environment over time, Fe will migrate to the surface preferentially over Ni to form a more thermodynamically stable Fe oxyhydroxide layer.[30]

3.4 Ligand binding

The calculated work surface functions for the bare mineral slabs are given in Supporting Information, SI11. Values obtained range from 4.38 eV (for the Fe terminated surface) to 4.80 eV (for the Ni terminated surface), with all other explicitly defined models falling between these two limits. Comparing to literature values, we note the experimental values of 4.67-4.81 eV for elemental Fe and 5.04-5.35 eV for elemental Ni.[42] Whilst acknowledging that the values are likely to differ for the mineral surface, the elemental values do at least show that our surface work functions are sensible numbers, if somewhat on the low side. This is likely an artefact of the pure DFT functional employed in this work, which is well known to over-delocalise d-electrons.[43] However we also note that values obtained from the LMTO tight binding approximation (5.54 eV for FCC Fe and 5.77 eV for FCC Ni)[44] appear to overcompensate for this shortcoming and return numbers that are too high.

Calculated binding energies for ethyl xanthate bound to Pn under both the VCA and atom-explicit (models 1-10) surfaces are given in Table 3. All total energies and work function values used to calculate these binding energies are presented in the Supporting Information, SI11. The VCA model

predicts a notably weaker energy than explicit model surfaces, which again suggests that its use is unreliable for pentlandite surface studies.

Considerable variations of the binding energy (*ca.* 130 kJmol^{-1}) were found across the range of explicit model surfaces. All recorded binding energies except one relate to a bridging geometry, with each of the sulfur atoms from the ligand coordinating to a separate metal on the mineral surface [see Figure 7(a)]. The only exception is model 2, which displays an energetically less favourable tripodal geometry, where one sulfur atom binds to two surface metals [see Figure 7(b)]. To observe whether there is a strong correlation between ligand binding energy and surface structure, the distribution of metals throughout the lattice was analysed as before. A breakdown of the metal site occupancies in each layer of surface models 1-10 is given in Table 3; ligand binding occurs onto layer 1.

Table 3 shows that, in general, Fe-enriched surfaces tend to have stronger binding energies to ethyl xanthate than Ni-enriched surfaces, and this trend is preserved if the work function correction is removed from the binding energy calculation (that is, the trend in binding energies is not simply a consequence of the variation in work function values). The two highest binding energies belong to systems where the ligand bridges two Fe ions, and conversely the weakest binding energy belongs to a system where the system bridges two Ni ions. To explore this further two [L+S] models were built in which the surface metal sites contained either all Fe or all Ni ions. The metal distributions, ligand binding energies and identities of the surface binding metal species for these models are given in the last two rows in Table 3 where 'Fe' (or 'Ni') denotes the Fe (or Ni) enriched surface model. These two models represent the upper and lower bounds of the range of ethyl xanthate binding energies, with just two exceptions. Model 2 has already been singled out as binding via a tripodal arrangement, preventing further comparisons. Model 1 has a lower binding energy than the Ni model and is the only model outside of the Ni-Fe range. Thus in general it would appear that with just two explicit-atom calculations an upper and lower ligand binding energy range can be established for a disordered mineral surface, with a high probability that most explicit models will lie between these two extremes.

Finally, the strain in the ligand and the surface which is associated with binding can be determined by running separate single point energy calculations of the ligand-bound and surface-bound geometries and comparing them with their optimised unbound counterparts. This suggests that, as would be expected, the ligand harbours more strain energy than the surface, with internal geometry changes corresponding to around 25 kJmol^{-1} of strain energy, versus around 8 kJmol^{-1} for the surface.

3.5 Hydration and hydroxylation enthalpies of Pn surfaces

The binding energies for increasing coverages of water molecules on the Fe- and Ni-enriched surfaces are presented in Table 4. Data relevant to the calculation of these binding energies is presented in the Supporting Information, SI11. The 'full' coverage monolayer model represents the lowest energy conformation achieved from the different repeat models outlined in the methodology. Also presented in Table 4 are the average binding energies per molecule at increasing surface coverage, to highlight whether hydrogen-bonding interactions between water molecules further stabilise the water layer as saturation of binding sites is reached, along with the binding energies for hydroxide on the Fe and Ni enriched surfaces. Geometric parameters for all three surface coverages on both surfaces are presented in the Supporting Information, SI12.

Optimised geometries obtained for the full water monolayer coverage Ni enriched and Fe enriched model are shown in Figure 8. The optimized models are very similar, showing only small geometric variations. The rotation of all but one of the water molecules in both models to address the surface hydrogen-atom 'down', as observed on the full monolayer models, was also observed on the 2/3 coverage models, whilst the 1/3 coverage model displayed an oxygen-atom 'down' orientation only. There is a marginal decline in average binding energy with increasing surface coverage, which we attribute to some water molecules adopting the less favourable hydrogen-atom 'down' geometry. In line with expecting the binding energy of a ligand to Pn to vary significantly between Ni- and Fe-enriched surfaces the hydration enthalpy for the Pn [111] surface changes from -165.4 to -193.9 $kJmol^{-1}$ for these surfaces, respectively.

The single molecule binding energy (1/3 coverage) for the Fe-enriched surface (-68.5 $kJmol^{-1}$) compares well with computational results from other iron containing sulfide minerals such as pyrite[45] (-54.1 $kJmol^{-1}$) and reconstructed chalcopyrite[46] (-95.4 $kJmol^{-1}$ which contains an additional water-surface hydrogen bond). No similar literature value could be found to benchmark the adsorption of water on millerite (NiS) or nickeline (NiAs).

Optimized models obtained for the binding of one OH^- anion to the Ni- and Fe-enriched Pn surface models are shown in Figure 9, for which the surface work function correction procedure returns a binding energy of -529.0 and -570.1 $kJmol^{-1}$, for the two surfaces, respectively. This is significantly higher than a monolayer of water and suggests the formation of covalent M-O bonds, which is also matched by geometric data showing Ni-O and Fe-O bond lengths of 1.808 and 1.778 Å, well within the range of M-O covalent bonding. A previous study by Jung *et al*[47] involving the binding of hydroxide to the Fe(100) surface (but without correcting for the negative charge) suggests a binding energy of an hydroxide group is -380 $kJmol^{-1}$. Removing the work function correction from the data obtained in this study resulted in the binding energies for the OH^0 fragment to the Ni and Fe enriched Pn surface

models falling to -342.2 and -423.6 kJmol^{-1}, respectively, which are comparable to the earlier literature value.

Comparing the relative binding strengths of water, hydroxide and ethyl xanthate to pentlandite gives an insight into the ease of collector uptake on the mineral surface, but bear in mind the binding energies have not been corrected for the effects of hydration. The modelling suggests that ethyl xanthate could easily displace even a full monolayer of water in order to bind. However the close binding energy values for xanthate and hydroxide suggest that the two will be in competition to address the mineral surface, a point confirmed by Klimpel[4848] . These results point to the need to carefully control pH conditions in the froth floatation process, which can be achieved through the addition of chemical modifiers.

4.0 Conclusions

In this study we conducted a first principles investigation into the mineral pentlandite (Pn), which exhibits positional disorder in relation to the Fe and Ni occupation sites. A cluster expansion expression suggests that lower energy bulk models were more likely to be constructed from lattices where the Fe and Ni ions are more heterogeneously dispersed, rather than like-ions clustered together. Further work will need to be undertaken to probe the likely distribution of oxidation states and spin states. The [111] Miller index, metal-terminated cleavage plane was identified to be a stable working surface and findings tentatively point towards the observation that more stable surfaces are generated when less Fe ions are present at the mineral surface. Virtual crystal approximation simulations were found to adequately reproduce bulk geometrical parameters, but could not reproduce the local surface distortions observed in the explicit surface models, and consequently produced a surface energy which is likely to be too low.

Surface work functions were determined in order to address the electron charge imbalance induced by introducing a negatively charged ligand to the mineral surface, thus permitting binding energies for anionic ligands on the Pn surface to be obtained. A range of energies (not corrected for the effects of solvation), from -447.9 kJ mol^{-1} (for a Pn surface with excess Ni at the interface) to –551.8 kJ mol^{-1} (for a Pn surface with excess Fe at the interface) were obtained, with values for most other random, explicitly-defined surfaces falling in between these two outer bracketed values. In an effort to quantify the effects of hydration on the mineral surface, binding energies of increasing surface coverage of water molecules (at 1/3, 2/3 and monolayer coverage) were calculated. Average binding energies per water molecule of *ca.* -55 and -65 kJ mol^{-1} for a Ni- and Fe-enriched surface respectively

were found. The binding energies of a lone hydroxyl anion to the two surface excess Pn models were found as -529.0 and -570.1 kJmol^{-1} for the Ni- and Fe-enriched surfaces respectively. These results indicate that while an ethyl xanthate collector could readily displace up to a full monolayer of water per unit cell in order to bind, it is likely that Fe-enriched surfaces will bind xanthate in competition with the hydroxide anion, whilst a Ni-enriched surface will preferentially bind hydroxide anions over xanthate. This work therefore highlights the need to use chemical modifiers to control pH conditions during the froth floatation process.

Acknowledgements

We acknowledge the UK Carr Parinello consortium for allocation of computing time on the ESPC high performance computing resource ARCHER (managed by the Edinburgh Parallel Computing Centre), the EaSTCHEM Research Computing Facility and the University of Edinburgh ECDF facility. We also acknowledge advice from Dr. D. S. Middlemiss (Warwick University), and invaluable support from Drs. Farinato, Nagaraj and Cocalia at CYTEC industries Inc. as well as Drs. Shackleton, Malysiak and Mr. De Vaux at Anglo American Plc., and to those companies for funding of a Ph.D. studentship for C.N.W. J. O. S. acknowledges the Engineering and Physical Sciences Research Council for the provision of a PhD. Studentship.

Figure 1. The full (a) and reduced (b) metal skeleton of the Pn bulk unit cell, with the octahedral sites (equivalent to 4 atomic positions) highlighted in purple, and the tetrahedral positions (32 atomic positions) highlighted in green. One atom (coloured yellow) has been selected at random to define the metal…metal $J_1 - J_5$ interactions and their lengths are shown in (b). (c) The lowest energy explicit model found for Pn from the cluster expansion process, showing just the Fe (shown in blue) and Ni (silver) ions in (d).

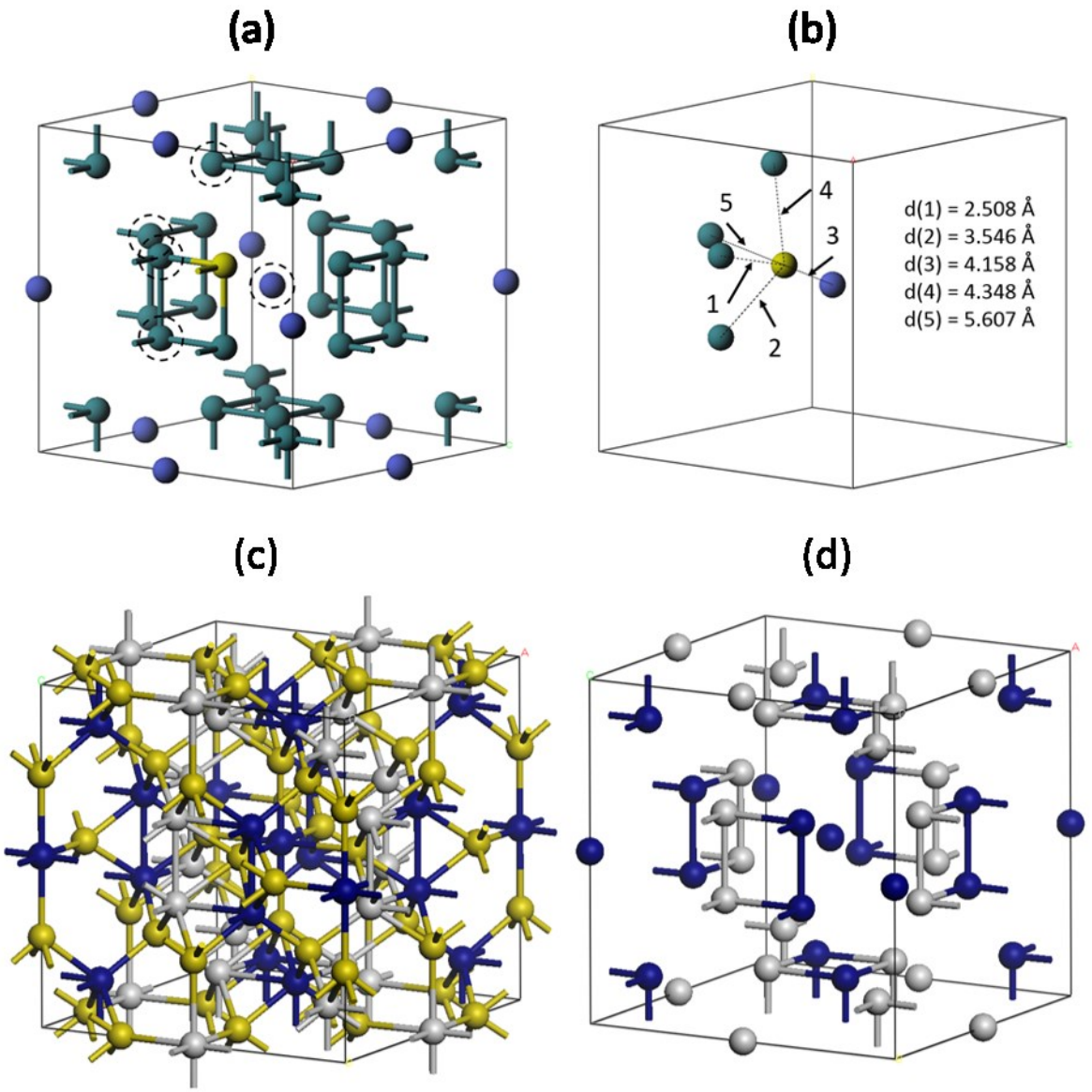

Figure 2. The favoured bridging geometry observed for ethyl xanthate binding to a Pn surface. For clarity the binding motif is shown in a 2 × 2 × 1 supercell. Legend: dark grey - carbon, yellow - sulfur, red - oxygen, white - hydrogen, light grey - nickel and blue - iron. The black line represents the periodic boundary.

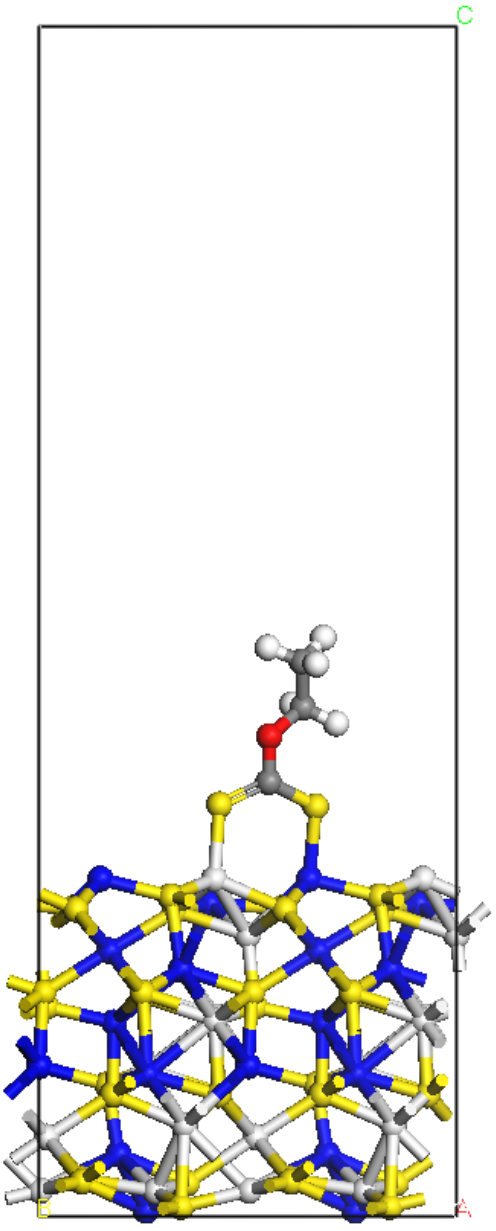

Figure 3. Side on (a) and top down surface net (b) of the [111] working surface of Pn. Legend: yellow – sulfur, purple - metal sites. Black lines represent periodic boundaries

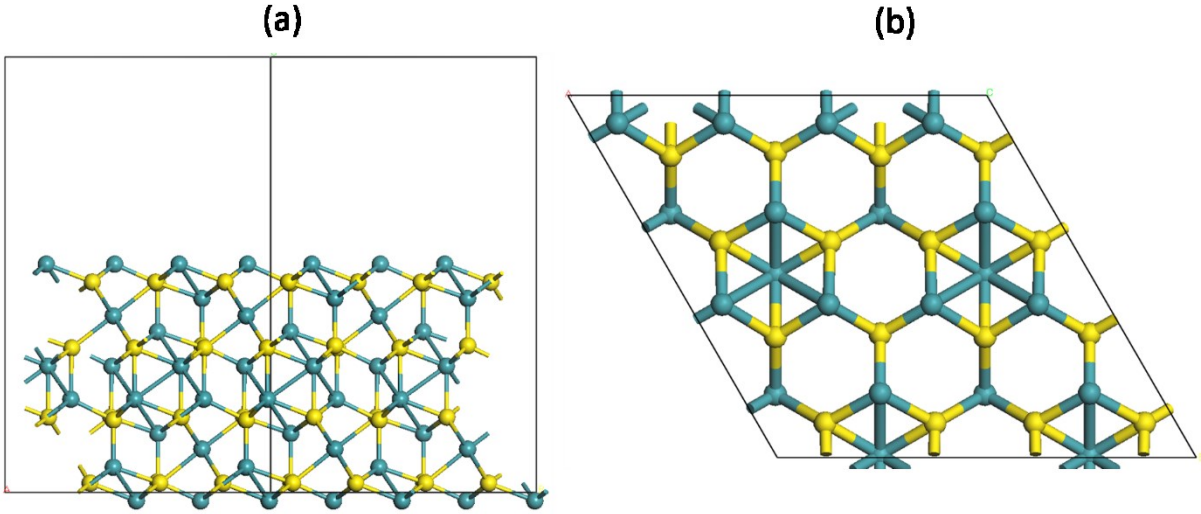

Figure 4. Correlation plot of actual total energy (derived from DFT calculations) versus predicted total energy (derived from the cluster expansion Hamiltonian) for the training set of explicit pentlandite bulk models (A-J), along with the lowest energy structure found by the cluster expansion approach (marked 'x').

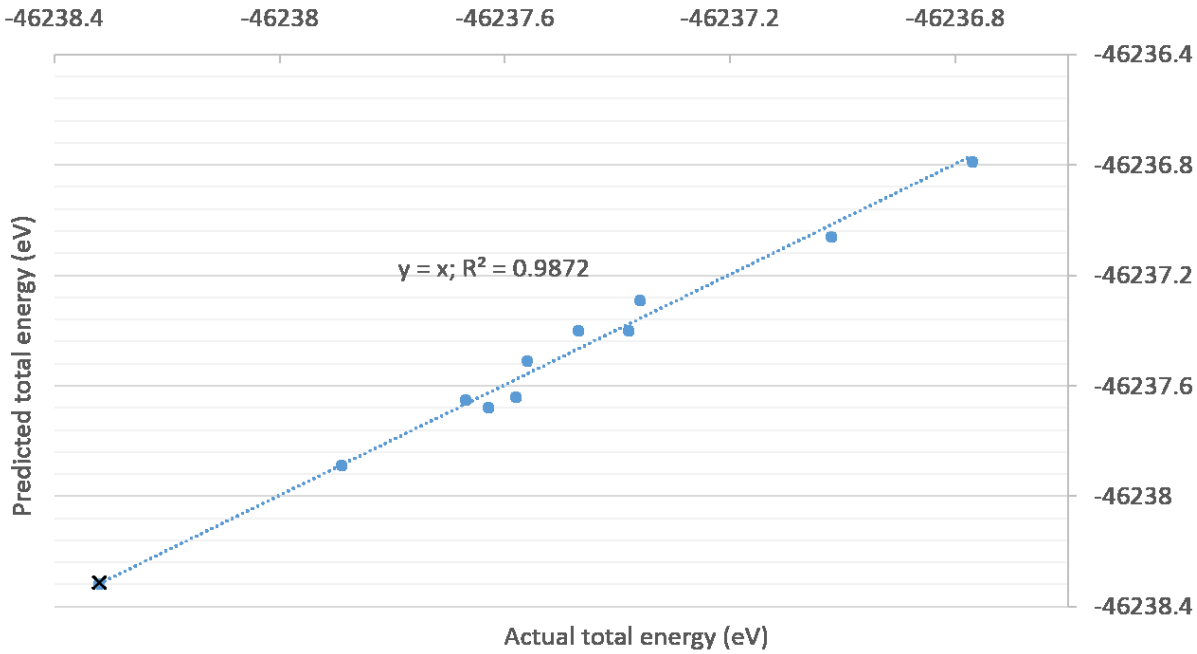

Figure 5. The average electrostatic potential along the *c* vector for the Pn slab unit cell, showing how V_{pot} is derived to calculate the surface work function (Φ_s).

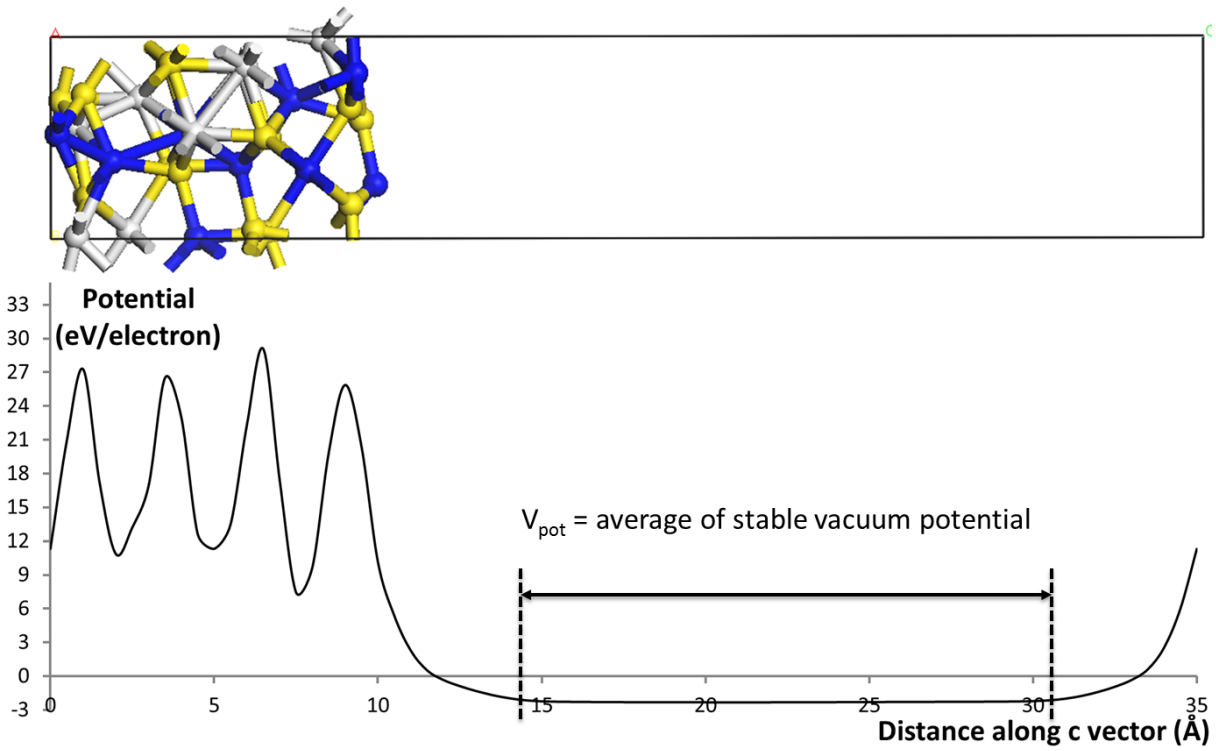

Figure 6. Comparison of optimised surface structures for the [111] Pn working surface, obtained by VCA and explicit (A-D) models. Legend: Yellow, blue and white are S, Fe and Ni respectively. Green atoms are mixed occupancy Fe/Ni VCA pseudoatoms. Periodic boundaries are omitted for clarity.

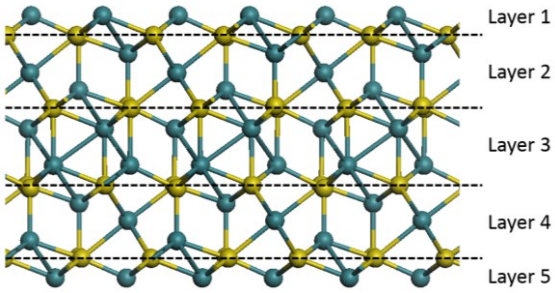

Pn VCA Surface

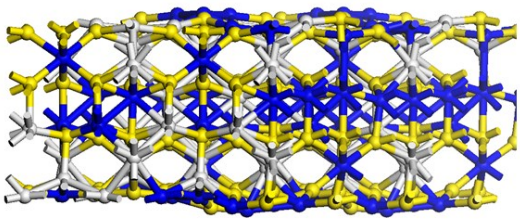

Pn Surface A

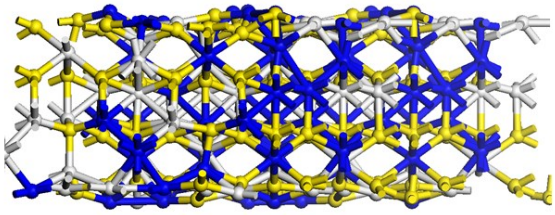

Pn Surface B

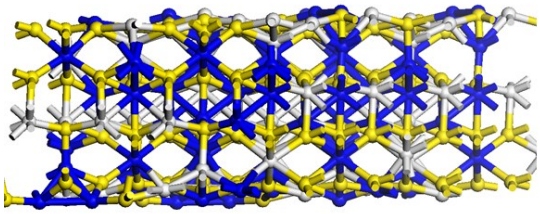

Pn Surface C

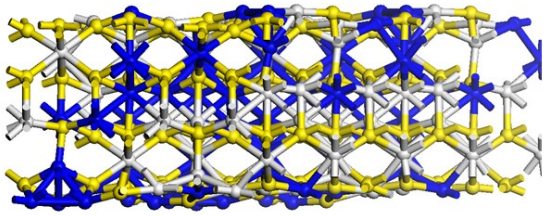

Pn Surface D

Figure 7. The recurrent bridging geometry (a) observed for all but one explicit [L+S] model and the less favourable tripodal geometry (b) observed for explicit model 2. Legend: dark grey - carbon, yellow - sulfur, red - oxygen, white (on ligand) - hydrogen, light grey (in lattice) - nickel and blue - iron.

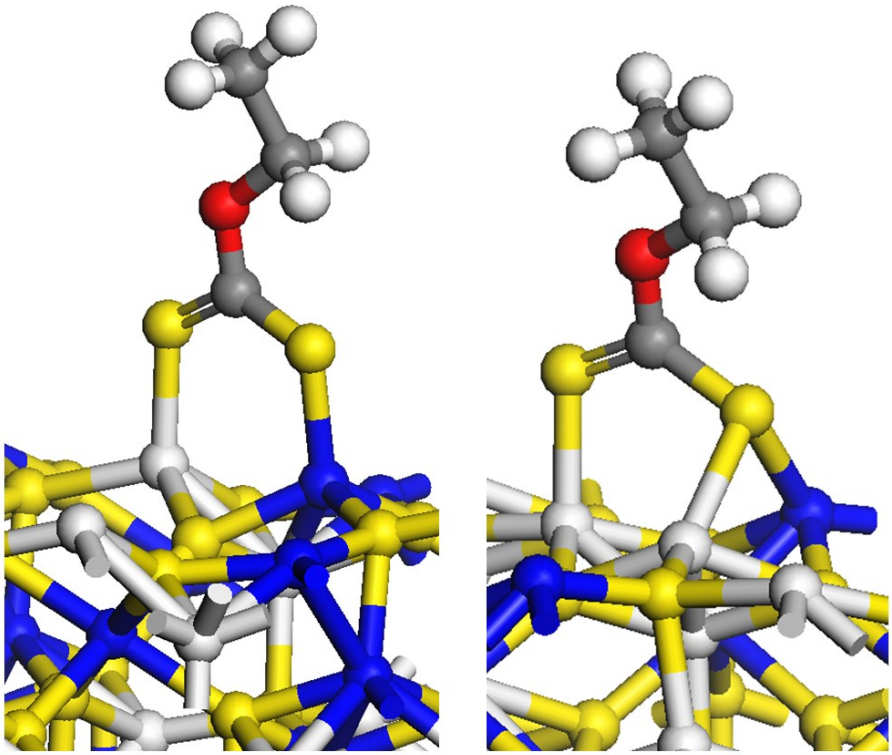

(a) (b)

Figure 8. Top-down (left) and side-on (right) views of the full surface coverage H_2O on Ni and Fe-enriched Pn surface models, showing the formation of a long range hydrogen bonding network. For clarity a 2 × 2 supercell is shown, and all subsurface ions have been removed. Legend: yellow – S, grey (in lattice) – Ni, blue (in lattice) - Fe, red – O, white (in ligand) – H, dashed black lines – H bonds

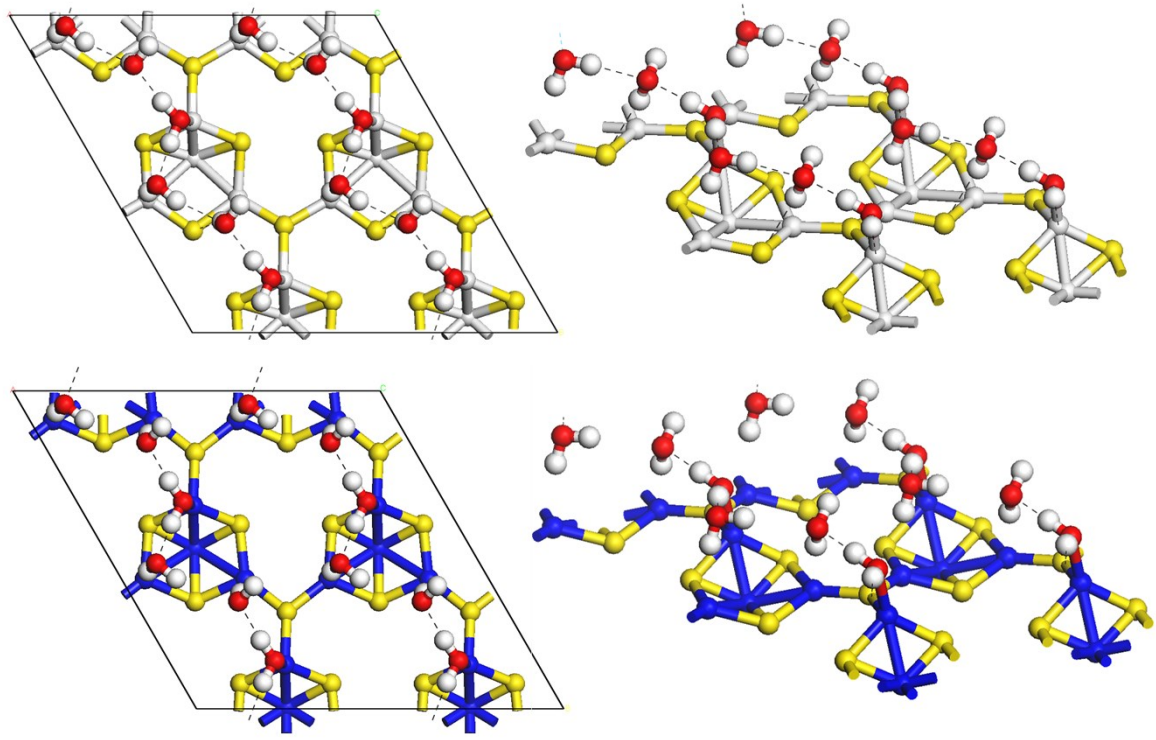

Figure 9. Top-down and side-on view of the 1/3 coverage OH Fe and Ni enriched Pn surface model. For clarity a 2x2 supercell is shown, and all subsurface ions have been removed. Legend: yellow – S, blue - Fe, grey (in lattice) – Ni, red – O, white (in ligand) – H,

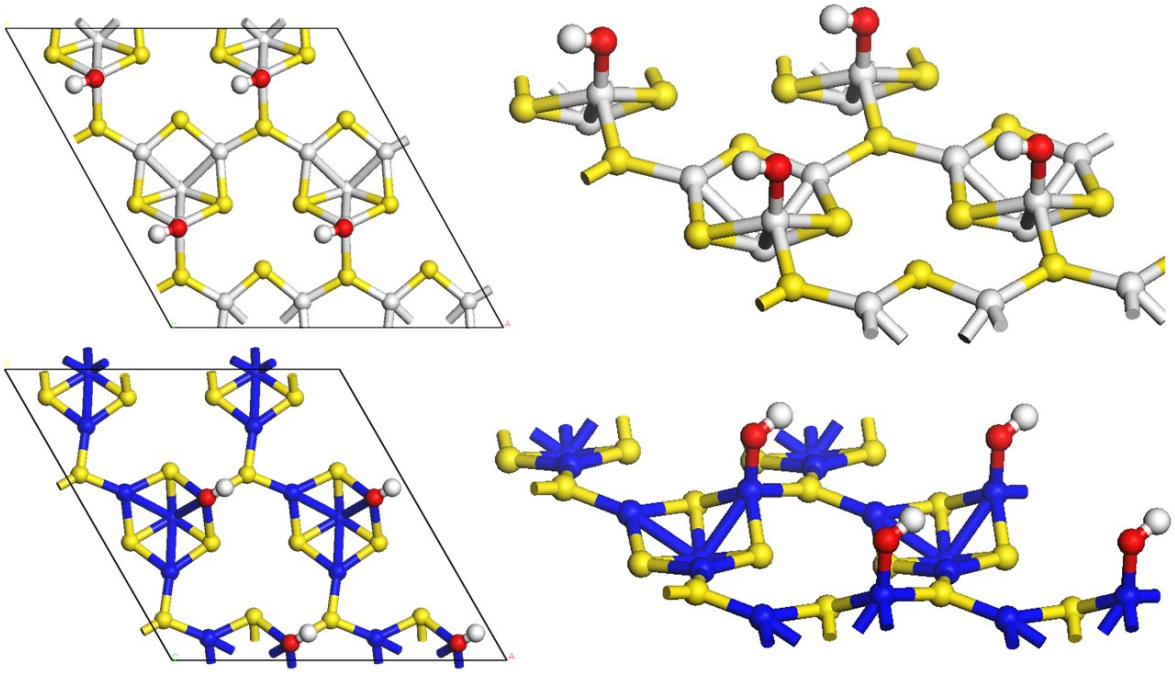

Table 1. Least squares fitted parameter values (and their respective errors) for E_0 and all J_n alongside the 'power ranking', defined as the J_n parameter multiplied by its degeneracy, as obtained from cluster expansion data for explicit models A-J.

Parameter	Parameter value (eV)	Error (+/-)	J_n Degeneracy	Power ranking
E_0	-46237.196	0.034	-	-
J_1	0.027	0.003	48	1.330
J_2	0.017	0.002	96	1.660
J_3	0.026	0.004	96	2.515
J_4	0.003	0.003	64	0.237
J_5	-0.004	0.001	192	-0.771

Table 2. Comparison of surface energies for VCA and explicit models of the Pn [111] working surface. The number of Fe and Ni ions are reported for each layer of each explicit slab model as "#Fe,#Ni". Values used in the calculation of the surface energy are presented in the Supporting Information, SI9.

Model	Layer 1 #Fe,#Ni	Layer 2 #Fe,#Ni	Layer 3 #Fe,#Ni	Layer 4 #Fe,#Ni	Layer 5 #Fe,#Ni	Surface energy (Jm^{-2})
VCA	12	12	24	12	12	0.58
A	6,6	3,9	16,8	3,9	8,4	1.34
B	7,5	6,6	12,12	6,6	5,7	1.20
C	4,8	8,4	10,14	8,4	6,6	1.13
D	5,7	5,7	13,11	5,7	8,4	1.20
E	6,6	6,6	12,12	6,6	6,6	1.17
F	5,7	7,5	11,13	7,5	6,6	1.17
G	4,8	6,6	12,12	6,6	8,4	1.16
H	6,6	7,5	11,13	7,5	5,7	1.19
I	3,9	6,6	12,12	6,6	9,3	1.17
J	4,8	7,5	11,13	7,5	7,5	1.14
C.E. Surf	6,6	6,6	12,12	6,6	6,6	1.38

Table 3. Comparison of VCA and randomised explicit model binding energies to ethyl xanthate and breakdown of each model layer occupancy. The number of Fe and Ni ions are reported for each layer of each explicit slab model as "#Fe,#Ni". Also shown are models with iron enriched and nickel enriched surfaces ("Fe" and "Ni" respectively in the first column). Total energies and related values used to calculate binding energy are presented in the Supporting Information, SI11.

Model	Binding energy ($kJmol^{-1}$)	Layer 1 #Fe,#Ni	Layer 2 #Fe,#Ni	Layer 3 #Fe,#Ni	Layer 4 #Fe,#Ni	Layer 5 #Fe,#Ni	Ligand bound To[a]
VCA	-318.1	3	3	6	3	3	Fe/Ni, Fe/Ni
1	-414.5	1,2	2,1	3,3	3,0	0,3	Ni, Ni
2	-437.1	1,2	1,2	3,3	2,1	2,1	-
3	-455.2	1,2	2,1	2,4	2,1	2,1	Fe, Ni
4	-466.6	1,2	2,1	4,2	1,2	1,2	Fe, Ni
5	-467.5	2,1	2,1	3,3	1,2	1,2	Fe, Ni
6	-481.4	1,2	2,1	3,3	2,1	1,2	Fe, Ni
7	-483.6	2,1	0,3	3,3	2,1	2,1	Fe, Ni
8	-488.3	2,1	1,2	3,3	2,1	1,2	Fe, Ni
9	-542.1	2,1	0,3	3,3	2,1	2,1	Fe, Fe
10	-543.1	2,1	1,2	2,4	3,0	1,2	Fe, Fe
Fe	-551.8	3,0	1,2	0,6	2,1	3,0	Fe, Fe
Ni	-447.9	0,3	2,1	6,0	1,2	0,3	Ni, Ni

[a] Metal species each sulfur atom in ethyl xanthate binds to, assuming a bridging geometry

Table 4. Binding energies of water molecules, hydroxide anions and neutral hydroxide fragments to Ni-enriched and Fe-enriched Pn surface models. Total energies and related values used to calculate binding energy are presented in the Supporting Information, SI11.

Pn Surface enrichment	Ligand	Surface coverage	Total binding energy of all ligands ($kJmol^{-1}$)	Average ligand binding energy ($kJmol^{-1}$)
Ni	H_2O	1/3	-46.7	-46.3
		2/3	-116.2	-57.8
		full	-165.4	-54.8
	OH^-	1/3	-529.0	-
	OH^0	1/3	-342.2	-
Fe	H_2O	1/3	-68.5	-68.1
		2/3	-131.9	-65.7
		full	-193.9	-64.3
	OH^-	1/3	-570.1	-
	OH^0	1/3	-423.6	-

References

1. Anthony, J. W.; Bideaux, R. A.; Bladh, K. W.; Nichols, M. C., *Handbook of Mineralogy*. Mineralogical Society of America: Chantilly, VA, 2003; Vol. 1.
2. Cabri, L. J., *Mineralogical Magazine* **1992,** *56*, 289-306.
3. Fuerstenau, M. C.; Jameson, G. J.; Yoon, R. H., *Froth Flotation: A Century of Innovation*. Society for Mining, Metallurgy, and Exploration: 2007.
4. Kawatra, S. K., Froth Flotation - Fundamental Principles. In *SME Mining Engineering Handbook*, Darling, P., Ed. Society for Mining, Metallurgy and Exploration: USA, 2011; pp 1517-1532.
5. Nagaraj, D. R., Minerals Recovery and Processing. In *Kirk-Othmer Encyclopedia of Chemical Technology*, J. Wiley & Sons, Inc.: 2005.
6. Sholl, D. S.; Steckel, J. A., *Density Functional Theory: A Practical Introduction*. J. Wiley & Sons: Hoboken, NJ, 2009.
7. Bellaiche, L.; Vanderbilt, D., *Phys. Rev. B.* **2000,** *61*, 7877-7882.
8. Iniguez, J.; Vanderbilt, D.; Bellaiche, L., *Phys. Rev. B.* **2003,** *67*, 224107.
9. Winkler, B.; Pickard, C. J.; Milman, C., *Chem. Phys. Lett.* **2002,** *362*, 266-270.
10. Leslie, M.; Gillan, M. J., *J. Phys. C.* **1985,** *18*, 973-1002.
11. Phatak, A. A.; Delgass, W. N.; Ribeiro, F. H.; Schneider, W. F., *J. Phys. Chem. C.* **2009,** *113*, 7269-7276.
12. Clark, S. J.; Segall, M. D.; Pickard, C. J.; Hasnip, P. J.; Probert, M. J.; Refson, K.; Payne, M. C., *Zeitschrift fur Kristallographie* **2005,** *220*, 567-570.
13. Perdew, J. P.; Burke, K.; Ernzerhof, M., *Phys. Rev. Lett.* **1996,** *77*, 3865-3868.
14. Vanderbilt, D., *Phys. Rev. B.* **1990,** *41*, 7892-7895.
15. Monkhorst, H. J.; Pack, J. D., *Phys. Rev. B.* **1976,** *13*, 5188-5192.
16. Pearson, A. D.; Buerger, M. J., *American Mineralogist* **1956,** *41*, 804-805.
17. Chichagov, A. V. Crystallographic and Crystallochemical Database for Minerals and their Structural Analogues. http://database.iem.ac.ru/mincryst/ (accessed 6/1).Referenceable?
18. Tenailleau, C.; Etschmann, B.; Ibberson, R. M.; Pring, A., *American Mineralogist* **2006,** *91*, 1442-1447.
19. Vaughan, D. J.; Ridout, M. S., *J. Inorg. Nucl. Chem.* **1971,** *33*, 741-746.
20. Drebushchak, V. A.; Fedorova, Z. N.; Sinyakova, E. F., *J. Therm. Anal. Calorim.* **1997,** *48*, 727-734.
21. Anisimov, V.; Zaanen, J.; Anderson, O. K., *Phys. Rev. B.* **1991,** *44*, 943-954.
22. Liechtenstein, A. I.; Anisimov, A. I.; Zaanen, J., *Phys. Rev. B.* **1995,** *52*, 5467-5470.
23. Leung, K.; Rempe, S. B.; Schultz, P. A.; Sproviero, E. M.; Batista, V. S.; Chandross, M. E.; Medforth, C. J., Density Functional Theory and DFT+U Study of Transition Metal Porphines Adsorbed on Au(111) Surfaces and Effects of Applied Electric Fields. *J. Am. Chem. Soc.* **2006,** *128*, 3659-3668.
24. Devey, A. J.; Grau-Crespo, R.; de Leeuw, N. H., *Phys. Rev. B.* **2009,** *79*, 195126-195133.
25. R. Woods; G. A. Hope; Brown, G. M., *Colloids and Surfaces A: Physiochem. Eng. Aspects* **1998,** *137*, 339-344.
26. M.K.G. Vermaak; P.C. Pistorius; Venter, J. A., *Miner. Eng.* **2005,** *18*, 575-584.
27. M. K. G. Vermaak; J. D. Miller; Lee, J., *Miner. Eng.* **2007,** *20*, 1337-1343.
28. Neugebauer, J.; Scheffler, M., *Phys. Rev,. B.* **1992,** *46*, 16067-16080.
29. Leeuw, N. H. d., Computer simulations of surfaces and interfaces: a case study of the hydration and dissolution of α-quartz SiO_2. In *Seminars of the Spanish Society of Mineralogy*, Prieto, M.; Brime, C., Eds. Spanish Society of Mineralogy: Madrid, 2008; Vol. 4.
30. Legrand, D. L.; Bancroft, G. M.; Nesbitt, H. W., *International Journal of Mineral Processing* **1997,** *51*, 217-228.
31. Makov, G.; C., P. M., *Phys. Rev. B.* **1995,** *51*, 4014-4022.
32. Lany, S.; Zunger, A., *Modelling Simul. Mater. Sci. Eng.* **2009,** *17*, 084002.
33. Woods, R., *J. Phys. Chem.* **1971,** *75*, 354-362.
34. Rusu, P. C.; G., G.; Brocks, G., *J. Phys. Chem. C.* **2007,** *111*, 14448-14456.

35. Inada, Y. Calculating Work Function using CASTEP. (COME OUT?)https://community.accelrys.com/servlet/JiveServlet/download/11552-7861/workfunction.pdf (accessed 7/1).
36. We generated models 1-10 rather than use the already defined explicit surface models A-J because, as binding energy calculations do not require comparison to an equivalent bulk model. We were therefore able to half the surface a and b vectors for models 1-10 compared to models A-J, saving on considerable computing expense.
37. Tomasi, J.; Mennucci, B.; 105, R. C., *Chem. Rev.* **2005**, 2999-3094.
38. Cheng, J.; Sprik, M., *Phys. Rev. B.* **2010,** *82*, 081406(R).
39. Michaelides, A.; Ranea, V. A.; Andres, P. L. d.; Kind, D. A., *Phys. Rev. Lett.* **2003,** *90*, 216102.
40. Carrasco, J.; Hodgson, A.; Michaelides, A., *Nat. Mater.* **2012,** *11*, 667-674.
41. Pezzullo, J. C. Least-squares non-linear regression web applet. http://statpages.org/nonlin.html (accessed 3/21). (COME OUT)
42. "Electron Work Function of the Elements", in CRC Handbook of Chemistry and Physics, 96th Edition (Internet Version 2016), W. M. Haynes, ed., CRC Press/Taylor and Francis, Boca Raton, FL. . **2005**.
43. Burke, K., Perspective on density functional theory. *Journal of Chemical Physics* **2012,** *136*, 150901-150909.
44. Skriver, H. L.; Rosengaard, N. M., *Phys. Rev. B.* **1992,** *46*, 7157-7168.
45. Stirling, A.; Bernasconi, M.; Parrinello, M., *J. Chem. Phys.* **2003,** *118*, 8917-8926.
46. Lima, G. F. d.; Oliveira, C. d.; Abreu, H. A. d.; Duarte, H. A., *J. Phys. Chem. C.* **2011,** *115*, 10709-10716.
47. Jung, S. C.; Kang, M. H., *Phys. Rev. B.* **2010,** (81), 115460.
48. Klimpel, R. R., *The Influence of Frother Structure on Industrial Coal Flotation*. Society for Mining, Metallurgy and Exploration: Littleton, CO, 1995; p 141-151.

Table of contents graphic